A SIMPLIFIED HYBRID METHODOLOGY FOR DETERMINING WELDING HEAT SOURCE PARAMETERS IN HIGH-STRENGTH STEELS

M. DADKHAH*, T. NITSCHKE-PAGEL*, K. DILGER*

**Institute of Joining and Welding (ifs), TU Braunschweig, Germany*

DOI 10.3217/978-3-99161-089-2-032, license CC BY 4.0

ABSTRACT

Welding simulations are critical for predicting the thermal and mechanical behavior of high-strength steels, as accurate thermal analysis, particularly under varying heat inputs, directly influences microstructure evolution and mechanical performance. Traditional heat source models rely on complex parameterization, often requiring variables that are computationally intensive or absent from standard material databases. This study addresses these limitations by introducing a simplified, hybrid methodology to determine heat source parameters for the Goldak's double ellipsoidal heat source model. The approach integrates various elements, including the molten pool's length components captured through high-speed videography (HSV), size of phase transformation zones, local temperature measurements combining with Design of Experiments (DOE), and finite element simulations. This integration aims to generate optimized parameters with enhanced accuracy and efficiency.

Three acceptance criteria were used to validate the optimized parameters derived from DOE: identical temperature gradients at thermocouple locations, equivalent macro-diagrams, and consistent cooling rates. These criteria ensured alignment between thermal analysis phase of the welding simulations and experimental data, facilitating robust calibration of heat source geometries and heat inputs. This framework significantly reduced computational costs compared to traditional trial-and-error calibration methods.

The results illustrate the capability of this method in predicting temperature distributions and related residual stresses afterwards. Furthermore, the adaptability of this methodology is a key strength, allowing it to be extended to other heat source models or different welding conditions. This versatility enhances its utility across a wide range of applications in welding research and industry, while its flexibility ensures that the methodology remains relevant as new materials and welding technologies emerge.

Keywords: welding simulation; heat source parameters; high-speed videography; DOE

INTRODUCTION

Welding simulations have emerged as essential tools for predicting and analyzing the complex thermal and mechanical phenomena that occur during welding processes. The significance of

these simulations becomes particularly pronounced in high-strength steel applications, where the intricate coupling between thermodynamic and mechanical properties necessitates precise control of process parameters to ensure optimal weld quality and structural integrity [1]. Beyond providing critical insights into thermal histories and mechanical performance of welded components, numerical simulations offer substantial economic advantages by reducing material waste, minimizing experimental trials, and optimizing manufacturing efficiency.

The Finite Element Method (FEM) represents the predominant computational framework for welding simulations, typically employing a sequential approach comprising thermal and mechanical analyses. The thermal analysis phase determines heat transfer mechanisms and temperature distributions throughout the welding path, which fundamentally govern microstructural evolution and subsequent mechanical properties of the weld zone. Subsequently, the mechanical analysis phase evaluates stress distributions, distortion and deformation patterns, as well as residual strain development during and after the welding process. This coupled thermo-mechanical approach enables comprehensive characterization of welding-induced material behavior, providing the foundation for systematic optimization of welding procedures [1,2].

Heat source modeling constitutes a critical component of thermal analysis within FEM-based welding simulations, serving to mathematically describe the generation and spatial distribution of thermal energy during welding operations. Established heat source models, including Goldak's double ellipsoidal (see Fig. 1) [3], employ sophisticated mathematical frameworks to simulate the three-dimensional and time-dependent distribution of heat input as the welding torch traverses the material. The accuracy of these heat source representations is paramount for capturing realistic temperature field evolution and subsequently predicting microstructural transformations and mechanical property development [4].

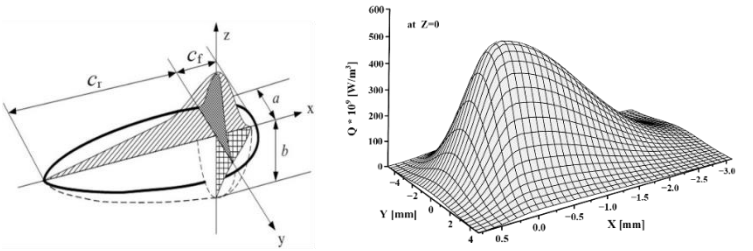

The double ellipsoidal volumetric heat source model (Goldak):

$$Q_{f,r}(x,y,z) = \frac{6\sqrt{3} f_{f,r} Q_A}{abc_{f,r}\pi\sqrt{\pi}} exp\left(-3\frac{x^2}{{c_{f,r}}^2}\right) exp(-3\frac{y^2}{a^2})\ exp\left(-3\frac{z^2}{b^2}\right)$$

The double elliptical surface heat source model (Li et al.):

$$Q_{f,r}(x,y) = \frac{6\, x_{f,r}\, Q_A}{a.\pi\,(C_f+C_r)} exp\left(-3\frac{x^2}{{c_{f,r}}^2}\right) exp(-3\frac{y^2}{a^2})$$

Fig. 1 Examples of well-established heat source models commonly employed in welding simulations [4,5]

The determination of appropriate parameters for heat source models presents considerable technical challenges in contemporary welding simulation practice. These parameters exhibit strong dependencies on material-specific thermophysical properties, including thermal conductivity, specific heat capacity, and temperature-dependent material behavior, as well as process-related variables such as heat input and welding travel speeds. For advanced materials, particularly high-strength steel alloys, the requisite parameter values are frequently unavailable in standard material databases or prove difficult to determine analytically due to complex thermo-mechanical coupling effects. Conventional approaches have predominantly relied on empirical trial-and-error methodologies or extrapolation from limited existing databases for parameter estimation. However, these traditional methods suffer from inherent limitations in both computational efficiency and prediction accuracy, while the scarcity of comprehensive material property databases further exacerbates the parameterization challenges [6].

This investigation addresses the aforementioned challenges through the development of a simplified hybrid methodology for heat source parameter determination. The proposed approach integrates molten pool geometry characterization and phase transformation zone analysis with experimental thermal history data, finite element simulations, and Design of Experiments (DOE) principles. This systematic framework enables efficient and accurate estimation of heat source parameters while minimizing dependence on empirical trial-and-error procedures and circumventing the need for extensive material property databases. Although the methodology is demonstrated through implementation with Goldak's double ellipsoidal heat source model, the underlying framework exhibits inherent versatility and can be readily adapted to other established heat source formulations [7]. The developed methodology aims to enhance welding simulation accuracy and reliability, ultimately contributing to improved weld quality prediction and manufacturing cost reduction.

MATERIALS AND EXPERIMENTAL SETTINGS

INVESTIGATED MATERIALS

Three steel grades were selected to evaluate the proposed methodology across different metallurgical complexities and thermal behaviors. HCT690T (TRIP700) represents a transformation-induced plasticity steel containing approximately 12% retained austenite in its initial microstructure, which undergoes strain-induced martensitic transformation under welding thermal cycles and mechanical loading. X40MnCrAlV-19 2.5 2 (TWIP) constitutes a highly alloyed twinning-induced plasticity steel with complex thermal properties and deformation mechanisms that present unique challenges for heat source parameter determination [8]. S355MC serves as a conventional microalloyed structural steel with well-established thermal behavior, providing a baseline reference for methodology validation.

These materials span a representative range of welding applications, from conventional structural applications to advanced automotive components, enabling comprehensive

assessment of the proposed heat source parameter determination approach. Table 1 presents the chemical compositions of the investigated materials.

Table 1 Chemical Composition of the Test Materials

S355MC

Mass fraction (%)	C	Mn	Si	P	S	Cu	Al	Nb	V	Ti
OBLF-Spec.	0.022	0.161	0.034	0.010	0.005	0.056	0.046	0.028	0.007	0.003

HCT690T

Mass fraction (%)	C	Mn	Si	P	S	Al	V	Cu	B	Ti+Nb	Cr+Mo
OBLF-Spec.	0.176	1.793	0.366	0.011	0.006	1.279	0.008	0.026	0.0001	0.022	0.02

X40MnCrAlV 19 2.5 2

Mass fraction (%)	C	Mn	Si	P	S	Al	Cr	Ti	V	Cu	Ni
OES-Spec.	0.377	18.62	0.246	0.019	0.0040	1.09	1.68	0.02	0.115	0.038	0.066

SAMPLE PREPARATION AND MATERIAL CHARACTERIZATION

Standard dog-bone tensile specimens were prepared for each alloy by waterjet cutting from metal sheets to ensure precise geometry and minimize heat-affected zones during preparation. Comprehensive mechanical property evaluation was conducted through tensile testing at ambient temperature and hot tensile testing across relevant temperature ranges to establish temperature-dependent material behavior. This experimental characterization provided essential baseline data for subsequent thermal and mechanical analyses in welding simulations.

Temperature-dependent thermophysical properties, including thermal conductivity, specific heat capacity, and thermal expansion coefficients, were determined using JMatPro software [9]. The computational framework employed HyperMesh for finite element mesh generation and ABAQUS with user-defined subroutine (DFLUX) for thermal analysis implementation [10]. The thermal model output served as input for subsequent phase transformation simulations, with Simufact Welding software utilized for enhanced computational efficiency and accuracy.

Phase transformation calculations were based on established kinetic models: the Johnson-Mehl-Avrami equation [11] for austenite and ferrite transformations during both heating and cooling cycles, and the Koistinen-Marburger equation [12] for martensitic phase fraction determination. The calculated phase fractions were subsequently employed to determine phase-specific strains and resulting deformations in the welded structure.

WELDING PROCESS

Tungsten Inert Gas (TIG) welding was employed to investigate the influence of thermal loading on heat source parameter determination. Bead-on-plate welds were performed without filler material addition, eliminating compositional variables and closely representing practical thin-plate welding applications such as overlap joints. Systematic variation of heat input was achieved by adjusting welding current and voltage while maintaining constant travel speed, enabling controlled investigation of the relationship between process parameters and heat source characteristics [13]. The specific welding parameters, corresponding heat input values, and associated cooling times ($t_{8/5}$) are presented in Table 2.

Table 2 Welding Parameters

Material	plate thickness [mm]	welding speed [cm/min]	voltage [V]	welding current [A]	heat input [kJ/cm]	$t_{8/5}$ [s]	in study name
S355MC	2	30	9.1	50	0.91	0.83	W01
			9.4	75	1.41	1.43	W02
			10.3	100	2.06	2.45	W03
			11.52	125	2.88	3.67	W04
			12.03	150	3.61	4.26	W05
HCT690T	1.75	30	9.1	50	0.91	1.84	W01
			9.4	75	1.41	2.49	W02
			10.3	100	2.06	3.06	W03
			11.16	112	2.50	3.66	W04
			11.52	125	2.91	4.32	W05
X40MnCrAlV 19 2.5 2	2	30	9.1	50	0.91	1.59	W01
			9.4	75	1.41	2.41	W02
			10.3	100	2.06	3.87	W03
			11.52	125	2.88	4.01	W04
			12.03	150	3.61	4.23	W05

shielding gas: 100% Ar / flow rate = 12 l/min

MOLTEN POOL CHARACTERIZATION

Real-time molten pool dynamics were investigated using high-speed videography at 5000 frames per second, coupled with CAILUX laser illumination to eliminate arc light interference and enable precise molten pool observation. Dimensional measurements of the molten pool were systematically recorded under varying welding parameters to characterize thermal behavior across the investigated materials.

To minimize measurement uncertainties associated with perspective distortions, dimensional analysis was conducted at a minimum of five discrete positions along each weld seam. Subsequently, only the length ratio between the front and rear sections of the molten pool was utilized for analysis, ensuring enhanced measurement reliability and data consistency, as illustrated in Fig. 2.

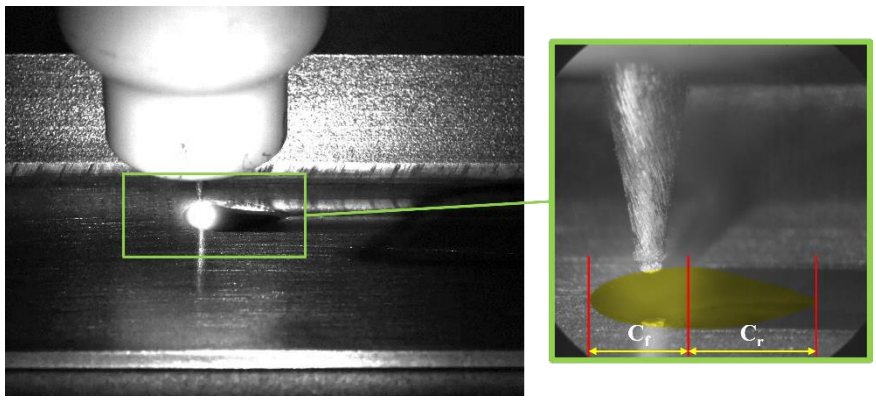

Fig. 2 Determination of molten pool dimensions using High-Speed Videography (HSV) technique

TEMPERATURE MEASUREMENT

Thermal gradients in the weld vicinity were monitored using a minimum of eight thermocouples positioned at strategic locations with 0.5 mm spacing intervals between adjacent sensors (See Fig. 3). Due to geometric constraints during thermocouple placement, they were distributed along the welding direction while maintaining minimal perpendicular distance to the weld path, optimizing temperature gradient resolution and data distribution quality.

The thermocouple data served as validation criteria for simulation results through direct comparison of both peak temperatures at specific locations and corresponding cooling rates. This experimental validation approach enabled quantitative assessment of the simulation accuracy and refinement of heat source parameters based on measured thermal histories.

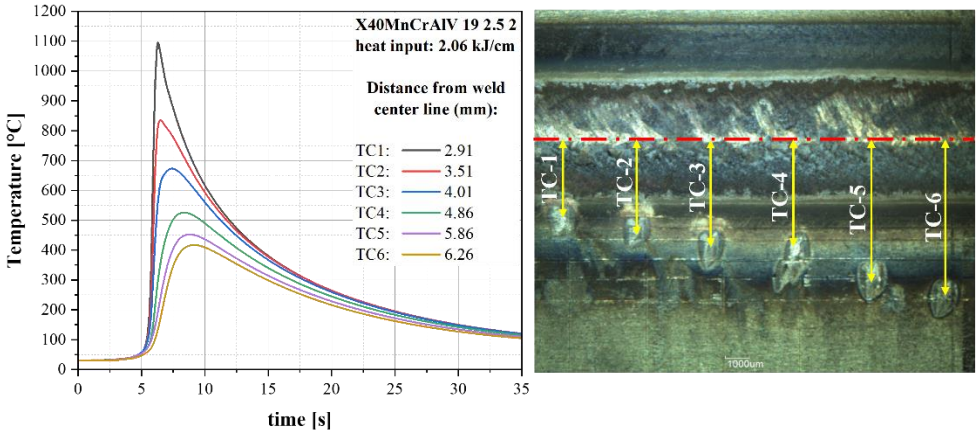

Fig. 3 Example of thermocouple attachment locations and their corresponding temperature history data for a specific heat input and material combination

METALLOGRAPHIC ANALYSIS

Heat-affected zone characterization was performed through systematic metallographic analysis of welded specimens. Cross-sectional samples were prepared using standard metallographic procedures, including mounting, polishing, and chemical etching, followed by digital image acquisition and analysis. This methodology enabled accurate measurement of weld zone macroscopic dimensions, as illustrated in Fig. 4. The quantitative metallographic approach facilitated parameter optimization by providing direct dimensional correlation between experimental measurements and computational model predictions, thereby validating simulation accuracy.

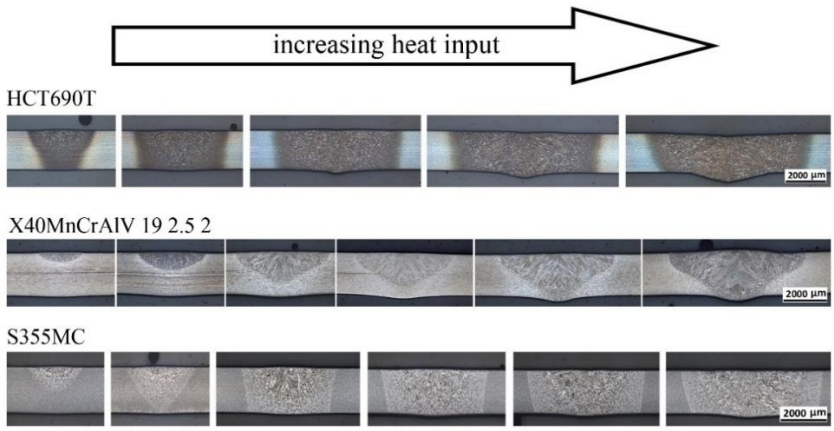

Fig. 4 Macroscopic metallographic morphology of welds examined under varying heat inputs

METHODOLOGY

This investigation employs the double ellipsoidal heat source model, commonly referred to as Goldak's model, to determine welding heat source parameters. The selection of this model is based on its demonstrated capability to accurately represent heat distribution in welding processes involving materials of significant thickness while maintaining computational efficiency through appropriate model simplification [5]. The methodology presented herein exhibits versatility and can be readily extended to alternative heat source models, including four ellipsoid quadrants or simpler configurations such as Gaussian surface flux models.

The mathematical formulation of Goldak's model is structured into two distinct regions: the front (f) and rear (r) sections of the heat source. Each region is characterized by a unique parameter set [14], enabling precise characterization of heat input dynamics and facilitating comprehensive understanding of temperature distribution throughout the weld zone.

Goldak's model represents a volumetric distributed heat source approach, which, according to established literature [5], is particularly suitable for thick specimen applications. However, this does not preclude its application to thin plate configurations, as demonstrated in the present study. For thin plate geometries, the primary consideration involves the depth parameter, which may introduce additional computational complexity and extend calculation time due to the inclusion of an extra variable in the solution procedure. Nevertheless, to demonstrate the model's capabilities and evaluate the influence of its implementation on final results, Goldak's model has been selected for this investigation.

The heat source intensity distribution is mathematically expressed as follows:

$$Q_{f,r}(x,y,z) = \frac{6\sqrt{3}\, f_{f,r}\, Q_A}{a\, b\, c_{f,r}\, \pi\sqrt{\pi}}\; e^{-3\left[\frac{x^2}{c_{f,r}{}^2} + \frac{y^2}{a^2} + \frac{z^2}{b^2}\right]} \tag{1}$$

$$Q_A = \eta . I . U \tag{2}$$

$$f_f + f_f = 2 \tag{3}$$

Equation (1) demonstrates the spatial distribution of heat through Gaussian-like exponential functions to represent anisotropic heat flux decay from the source in both front and rear sections. Equation (2) defines the total heat input (Q_A), establishing the relationship between arc efficiency (η), welding current (I), and voltage (U), thereby quantifying the total power input into the welding process. Equation (3) ensures proper distribution of the total heat input between the two ellipsoidal regions while maintaining consistency with the model's mathematical formulation [3].

The aforementioned equations reveal seven unknown parameters - $a, b, c_f, c_r, f_f, f_r,$ and η - that require determination to accurately solve the heat source model equations. Resolution of these parameters is essential for computing heat quantities at each nodal position within the meshed simulation model. The present study aims to simplify or eliminate as many unknown parameters as possible from the heat source equations, thereby streamlining the computational process and enhancing the model's practical applicability across diverse welding scenarios.

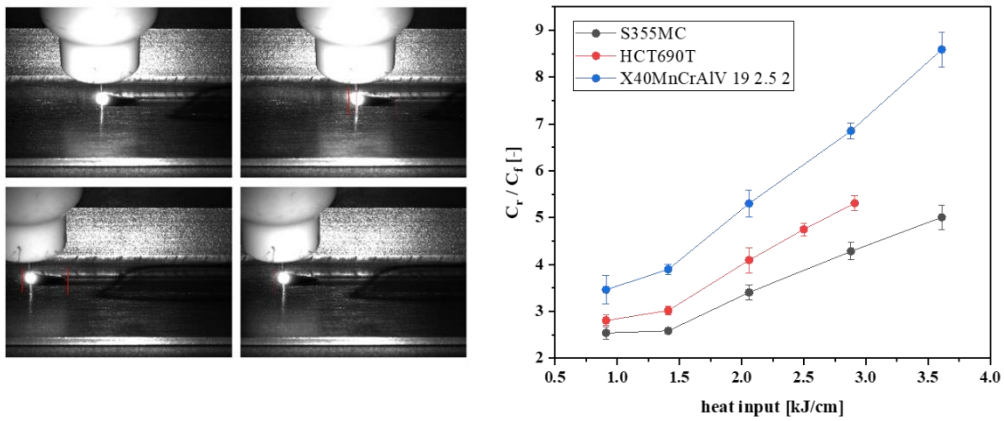

Fig. 5 Relative length ratio of the molten pool formation during welding process as captured by High-Speed Videography (HSV) system

As described in the experimental setup, High-Speed Videography (HSV) was employed to examine the length ratio of the molten pool across all welding parameters investigated. This technique enabled precise assessment of molten pool dimensions in relation to heat source dynamics. To minimize measurement errors resulting from perspective distortions in the acquired images, molten pool length ratios were measured at a minimum of five different positions for each condition. The results of these measurements are presented in Fig. 5. Based on this analysis, one parameter (c_f or c_r) can be determined as a function of the other, as expressed in the following relationship:

$$c_r = c_f \times \frac{c_r}{c_f} \tag{4}$$

Furthermore, the fraction of heat flux distributed to the front and rear halves of the heat source can be related to the length components and their ratio through the following equations [3,6]:

$$f_f = \frac{2\,c_f}{c_f + c_r} \quad , \qquad f_r = \frac{2\,c_r}{c_f + c_r} \tag{5}$$

Utilizing the length ratio values obtained from HSV analysis of the molten pool history in conjunction with the aforementioned equations enables effective reduction of the model's unknown parameters from seven to four: a, b, c_f $(or\ c_r)$ and η. In the subsequent phase, the remaining parameters must be determined such that the heat source mathematical equation yields accurate solutions.

This study proposes the application of Design of Experiments (DOE) to systematically solve the welding heat source model equations with four input factors corresponding to the remaining unknown parameters. A fundamental prerequisite for this approach is establishing unity in the responses measured across different factor levels defined within the DOE framework.

This unity requirement implies that outputs obtained from the DOE must remain directly comparable when utilizing various combinations of factor levels. However, a significant

challenge emerges because varying these input parameters results in the formation of distinct weld geometries, including the Fusion Zone (FZ), where temperatures reach or exceed the liquidus temperature; the Partial Melting Zone (PMZ), where temperatures range between solidus and liquidus temperatures; and the Heat Affected Zone (HAZ), characterized by temperatures at or above the austenitization point, as illustrated schematically in Fig. 6.

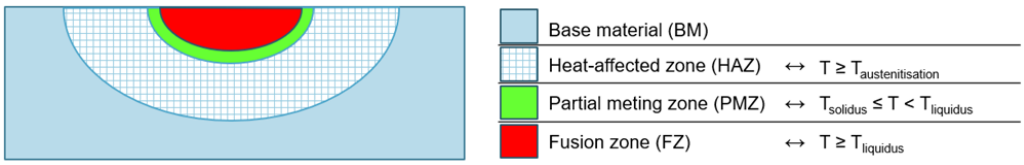

Fig. 6 Solid-state phase transformation zones in welded specimens, illustrating the distribution of FZ, PMZ, and HAZ

Consequently, these geometries and their corresponding temperatures at specific coordinates within the welded specimens become inherently non-comparable when different input factor levels are employed.

To address this challenge, the consistency of temperature limits governing these transformation zones can be utilized. The boundaries of these zones maintain constant temperature conditions across varying scenarios. For instance, the boundary of the Fusion Zone is defined by the liquidus temperature, the Partial Melting Zone extends from the solidus temperature to the liquidus temperature, while the Heat Affected Zone boundary corresponds to the austenitization temperature for ferritic steels [2].

Based on varying input factor levels and heat input quantities, three distinct types of transformation zone geometries can form, all of which align closely with metallographic observations [15].

Fig. 7 presents a visual representation of transformation zone widths on the welding surface, captured through metallographic analysis. These images clarify the specific geometry expected for a given heat input, grounding the study in empirical observations and enabling meaningful comparisons with simulation results. It should be noted that the Fusion Zone (FZ) and Heat Affected Zone (HAZ) are utilized for TRIP and S355MC steel, whereas for TWIP steel, the FZ and Partial Melting Zone (PMZ) are considered, since TWIP steel does not undergo phase transformation that defines an austenitization temperature due to its fully austenitic structure [16].

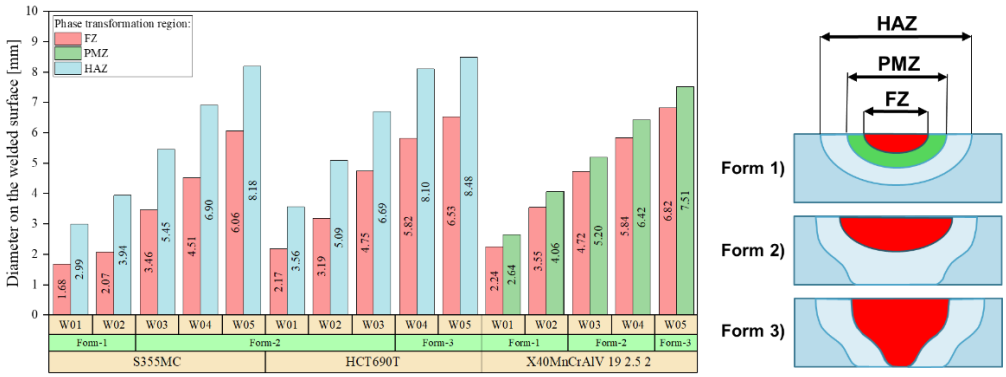

Fig. 7 Geometry of phase transformation areas utilized in Design of Experiments (DOE) for welded specimens, showing variations in transformation zone morphology corresponding to different heat input levels and resulting weld profiles

Utilizing the data presented in Fig. 7, distinct DOE frameworks can be developed for each heat input level and material investigated. In these experimental designs, the unknown parameters of the heat source model serve as input factors, while the responses are represented by maximum temperatures attained at phase change boundaries. The solution to this DOE is determined by minimizing the temperature difference at phase change boundaries - defined by liquidus, solidus, or austenitization temperatures - between the simulated model and theoretical values. This approach ensures alignment between the model's predictions and expected thermal thresholds. Fig. 8 illustrates one of the DOE system responses for a specific heat input, calculated using simulation data.

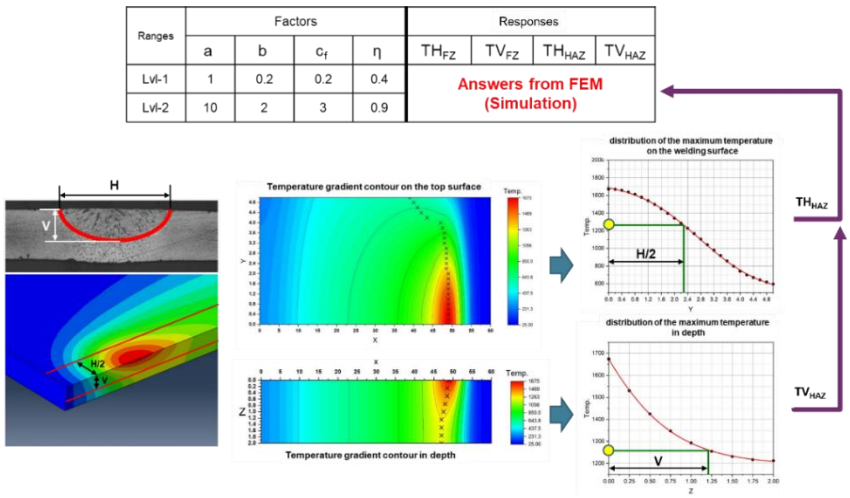

Fig. 8 Example of response extraction from simulation model for DOE variation based on defined factor settings

The number of simulations required to achieve highly accurate results from the DOE system depends on the complexity of the selected model. In this study, a fifth-order model was chosen to provide a reasonable balance between computational effort and accuracy. This choice was particularly advantageous given the high simulation speed afforded by the selected double ellipsoidal heat source model, ensuring efficient yet precise analysis.

It should be noted that multiple numerical solutions can be obtained in such DOE systems based on the constraints defined in the solution selection procedure. In the subsequent phase, the most appropriate optimal parameters must be identified. To evaluate solutions and select the optimal answer, the following conditions have been established to compare the simulation model with experimental data:

- **Maximum peak temperature similarity at the location of attached thermocouples**: This criterion ensures that simulated temperatures in welding phase at thermocouple sites correspond accurately with experimental measurements. This alignment validates the simulation's heat distribution accuracy, thereby enhancing reliability for optimal welding parameter selection.
- **Maximum similarity of the formed transformation area in cross-section of metallographic macrodiagram**: This condition ensures that the size of the phase transformation zones in the simulation corresponds closely to the macroscopic metallographic images observed around the weld zone, enhancing the model's physical accuracy.
- **Temperature gradient similarity on the welding surface during the cooling phase**: This criterion demands that the simulated temperature gradient during cooling corresponds with experimental data. For reaching an appropriate result, the convection and radiation factors which reflect the environmental or experiment setup constraints should be defined correctly.

By adhering to these conditions, the analysis aims to refine the selection of optimal parameters, thereby improving the reliability and precision of the simulation outcomes.

RESULTS AND DISCUSSION

The application of the design of experiments (DOE) approach to the Goldak's energy equation typically yields multiple mathematically valid solutions under the established boundary conditions. The selection of the most physically meaningful solution requires systematic evaluation based on the criteria outlined in the methodology section.

For validation of the thermal behavior during the heating phase, the maximum surface temperature at thermocouple locations relative to the weld centerline serves as the primary reference parameter. Given the dense array of thermocouples positioned at predetermined distances from the specimen surface, the optimal solution is identified as that which produces maximum temperature values and thermal distributions most closely corresponding to the experimental measurements at equivalent locations (Fig. 9).

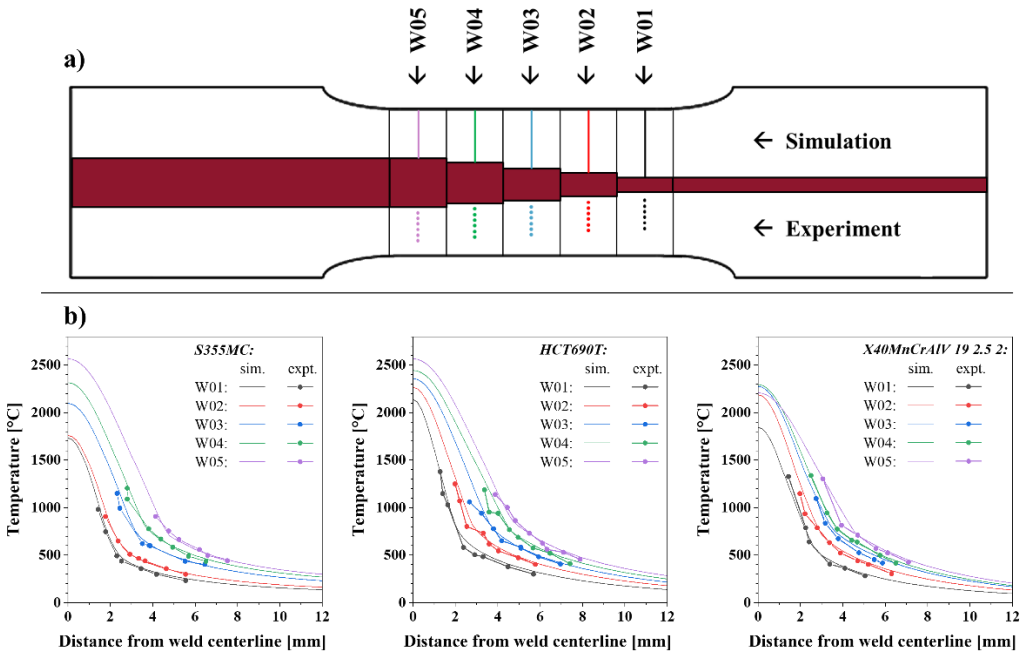

Fig. 9 a) Schematic representation of welded specimen under heat input variation showing thermocouple locations and simulation temperature measurement areas around the centreline perpendicular to the median axis, b) corresponding distribution of peak temperatures at various distances from the weld centreline for both experimental and simulation results across all investigated materials

During the cooling phase, the austenite transformation to martensite, bainite, pearlite, or ferrite phases is governed by the cooling time $t_{8/5}$ [17]. The cooling behavior is significantly influenced by environmental test conditions, including ambient temperature, fixture geometry, and thermal contact conditions. In the numerical model, these factors are incorporated through appropriate film coefficients and radiation parameters at the interfaces between the specimen and supporting fixtures or ambient air.

The numerical simulation parameters were calibrated to ensure that both the calculated cooling time and residual heat content after a specified time interval matched the experimental values within acceptable tolerances. Following this calibration procedure, the computed temperature gradients from the thermal simulation demonstrated excellent correlation with experimental data, as exemplified in Fig. 10. This high degree of accuracy in temperature prediction is critical for subsequent mechanical analyses, which require precise thermal history data throughout the entire cooling cycle [18,19].

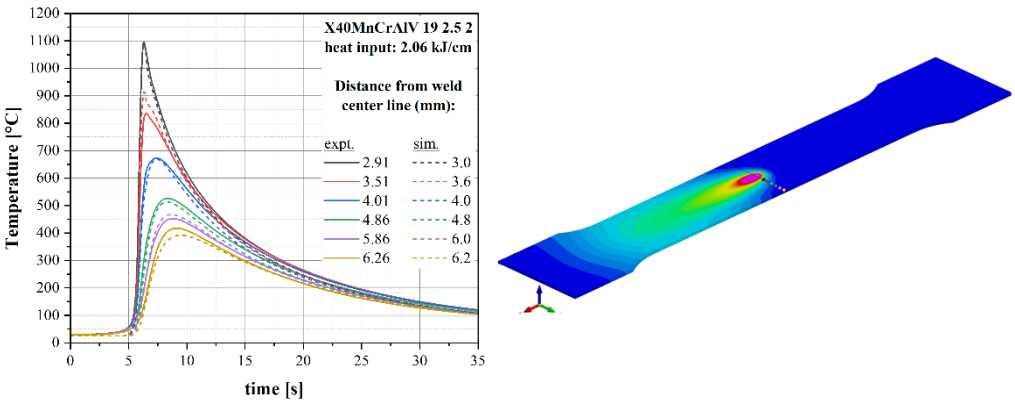

Fig. 10 Example of a calibrated thermal analysis model showing thermal history at nodes nearest to thermocouple locations on the specimen surface for a specific heat input and material

The comparison between calculated molten pool geometries derived from thermal simulations and metallographic cross-sections demonstrates excellent agreement, as illustrated in Fig. 11. Across all investigated materials, the simulated weld pool dimensions closely correspond to experimentally observed geometries under varying heat input conditions. This consistent correlation between numerical predictions and experimental observations confirms the accuracy and reliability of the simulation methodology in reproducing the physical phenomena of the welding process [20]. The strong agreement between computational and metallographic results validates both the parameter selection procedure and demonstrates the robustness of the heat source model in accurately capturing the thermal distribution and geometric characteristics of the molten pool formation.

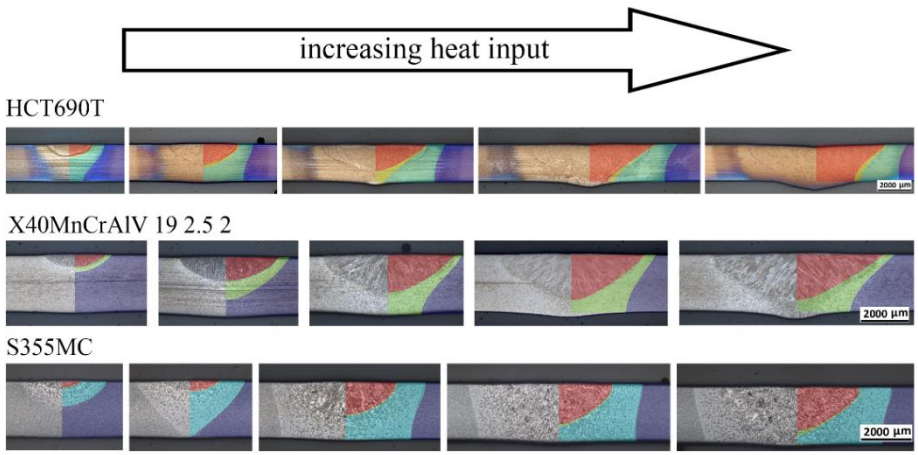

Fig. 11 Comparison of molten pool geometries obtained from thermal simulation with corresponding metallographic cross-sections

For validation purposes, different temperature criteria were applied based on material characteristics. For S355MC and HCT690T steels, phase transformation boundary temperatures in both the fusion zone (FZ) and heat-affected zone (HAZ) were considered as comparison parameters. However, for the austenitic steel X40MnCrAlV 19-2.5-2, the temperature at the FZ and partially melted zone (PMZ) boundary was utilized due to its distinct metallurgical behavior. In cases where significant discrepancies between simulation and experimental results exceed acceptable tolerances, alternative parameter sets from the DOE matrix are systematically evaluated.

Following the application of validation criteria to identify optimal parameters from the DOE solutions, the unknown heat source model parameters were determined for all investigated materials, as presented in Fig. 12.

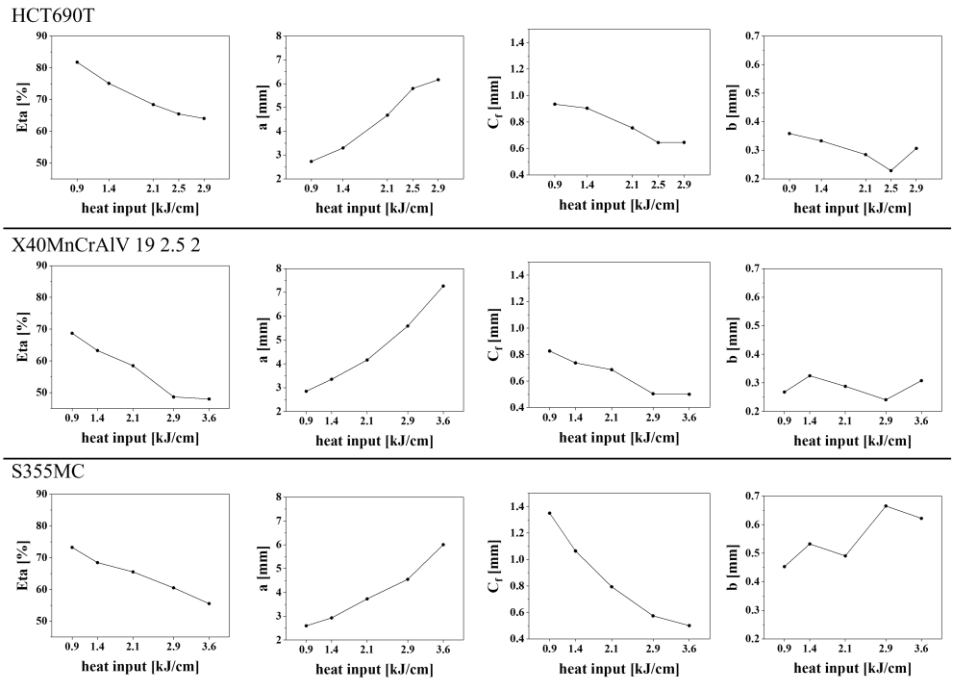

Fig. 12 Distribution of determined heat source parameters across varying heat input levels for all investigated materials

The results demonstrate that increasing heat input produces elevated temperatures within the welding zone, as previously shown in Fig. 9, which correspondingly increases molten pool dimensions. This relationship is clearly reflected in the distribution of parameter *(a)* across varying heat input conditions. A notable characteristic observed across all parameters is their approximately linear response to heat input variations.

Of particular significance is the behavior of the efficiency factor, which exhibits a decreasing trend with increasing heat input. This finding contradicts the common assumption

in many welding studies where efficiency is treated as a constant value for a given welding process, highlighting a deviation from observed physical behavior. The distribution of parameter *(b)* remains relatively constant across all heat input conditions, suggesting that the depth parameter may be omitted from the heat source equation for thin plate welding applications. This observation indicates that a double elliptical surface heat source model could yield comparable accuracy while reducing computational complexity by eliminating one unknown parameter, thereby requiring fewer simulation runs in the DOE framework.

The parameter (C_f) demonstrates a decreasing trend with increasing heat input, which can be attributed to the specific experimental boundary conditions and fixture constraints under which molten pool geometries were measured during welding. This suggests that alternative clamping systems and constraint configurations may influence this parameter, as well as other heat source parameters, emphasizing the importance of considering experimental setup conditions in parameter determination.

As discussed in the previous section, these determined parameters enable the calculation of remaining heat source model equation parameters for each specific heat input condition through the application of equations (1-5).

The thermal analysis results serve as input data for the subsequent mechanical analysis in the welding simulation procedure. Residual stress represents one of the most critical mechanical characteristics that can be determined through this approach, as its distribution across the welded surface significantly influences mechanical performance and structural integrity. In this investigation, the computed residual stresses from the simulation model were validated against experimental data obtained through X-ray diffraction (XRD) measurements [21].

Fig. 13 presents the residual stress distributions corresponding to specific heat input conditions for each investigated material. The simulation-predicted stress profiles are directly compared with experimentally measured data within each diagram. The strong correlation between these profiles demonstrates the reliability of the simulation methodology based on the heat source parameters determined in this study.

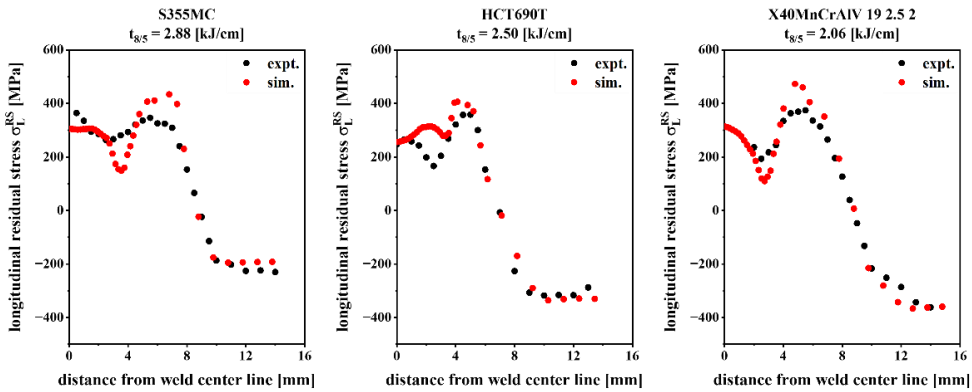

Fig. 13 Distribution of residual stress corresponding to specific heat input levels in the investigated materials

For the numerical calculation of residual stresses, an isotropic hardening model was implemented. This constitutive model assumes uniform hardening behavior throughout the material, thereby simplifying the computational process while maintaining satisfactory correlation with experimental observations. However, the isotropic hardening assumption may not fully capture the complexities of material behavior during phase transformations, particularly within the fusion zone, or under more demanding loading scenarios. Future investigations could incorporate alternative hardening models, such as kinematic or combined hardening approaches, to assess potential improvements in residual stress prediction accuracy. Through the implementation of a broader range of constitutive models, the proposed methodology could be further refined, potentially expanding its applicability to diverse materials and welding conditions.

CONCLUSION

This investigation presents a simplified methodology for determining welding heat source parameters specifically developed for high-strength steel applications. The implementation of a double ellipsoidal volumetric heat source model successfully captured the thermal characteristics of the welding process, enabling accurate simulations while avoiding the computational complexities typically associated with conventional approaches. The systematic integration of high-speed videography (HSV), metallographic macrostructure analysis, variable heat input conditions, strategically positioned thermocouple arrays, and design of experiments (DOE) methodology provided an effective framework for identifying optimal heat source parameters with enhanced efficiency and precision.

A fundamental aspect of this methodology is the utilization of unified response criteria within the DOE framework for specific welding configurations. The DOE approach facilitated systematic exploration of parameter combinations, yielding optimized solutions with high consistency in responses, particularly at phase transformation boundary temperatures. Stringent validation criteria ensured excellent agreement between simulation results, metallographic observations, and experimental temperature measurements.

The reliability of the simulation model was further confirmed through accurate prediction of residual stress distributions, as validated by X-ray diffraction (XRD) measurements. This validation demonstrates the model's capability to capture the complex thermal and mechanical phenomena occurring in welded specimens, establishing a robust foundation for future developments in welding simulation technology.

Future enhancements to this methodology could include parameter recalibration for varying welding speeds and heat input ranges, thereby extending the model's applicability. Additionally, investigation of alternative constitutive models, such as kinematic or combined hardening approaches, may provide enhanced understanding of material behavior and improve residual stress prediction accuracy across diverse welding scenarios. Potential research directions include studies on welding under different constraint conditions, such as alternative fixture designs or clamping systems, as well as investigation of the effects of pre-deformation on welding behavior and subsequent material properties.

This work provides a significant simplification of welding simulation procedures, offering a practical and efficient computational tool for researchers and engineers focused on welding process optimization and advancement of high-strength steel joining technologies.

ACKNOWLEDGEMENTS

The results presented in this study were achieved as part of a collaborative effort between the Technical University of Braunschweig and the Karlsruhe Institute of Technology, supported by the German Research Foundation (DFG) under project numbers Gi376/17-1 and Ni508/19-1. The authors gratefully acknowledge the financial support provided by the German Research Foundation.

References

[1] LARS-E LINDGREN: *Computational Welding Mechanics: Thermomechanical and microstructural simulations*, Woodhead Publishing, 2007.

[2] J. SUN: *Influence of heat input model parameters on the simulated properties in ferritic steel weldments*, 2019.

[3] J. A. GOLDAK, M. AKHLAGHI: *Computational Welding Mechanics*, Physica-Verlag, 2005.

[4] Z. SATERNUS: 'Computer Methods for Determination of Deformations in Welded Closed Profiles', *Procedia Engineering*, 177, pp. 188-195, 2017.

[5] E. J. G. NASCIMENTO, E. DOS SANTOS MAGALHÃES, L. E. DOS SANTOS PAES: 'A literature review in heat source thermal modeling applied to welding and similar processes', Int. J. Adv. Manuf. Technol., 126, pp. 2917-2957, 2023.

[6] S. TRUPIANO, V. G. BELARDI, P. FANELLI, L. GAETANI, F. VIVIO: 'A semi-analytical method for the calculation of double-ellipsoidal heat source parameters in welding simulation', IOP Conf. Ser.: *Mater. Sci. Eng.*, 1214, 12023, 2022.

[7] V. GARCÍA-GARCÍA, I. MEJÍA, F. REYES-CALDERÓN: 'Improved thermal FE numerical model/DoE based on the Taguchi method to estimate weld penetration/energy and non-metallic inclusions: a case study in Ti-containing TWIP steel butt joints', *Int. J. Adv. Manuf. Technol.*, 105, pp. 101-120, 2019.

[8] O. BOUAZIZ, S. ALLAIN, C. P. SCOTT, P. CUGY, D. BARBIER: 'High manganese austenitic twinning induced plasticity steels: A review of the microstructure properties relationships', *Current Opinion in Solid State and Materials Science*, pp. 141-168, 2011.

[9] N. SAUNDERS, U. K. Z. GUO, X. LI, A. P. MIODOWNIK, J.-P. SCHILLÉ: 'Using JMatPro to model materials properties and behavior', *JOM*, 55, pp. 60-65, 2003.

[10] N. AN, G. YANG, K. YANG, J. WANG, M. LI, J. ZHOU: 'Implementation of Abaqus user subroutines and plugin for thermal analysis of powder-bed electron-beam-melting additive manufacturing process', *Materials Today Communications*, 27, 102307, 2021.

[11] W. A. JOHNSON and R. F. MEHL: *Reaction Kinetics in Processes of Nucleation and Growth*, pp. 416-442, 1939.

[12] D. P. KOISTINEN, R. E. MARBURGER: 'A general equation prescribing the extent of the austenite-martensite transformation in pure iron-carbon alloys and plain carbon steels', *Materials Science Engineering*, pp. 365-378, 1959.

[13] M. BJELIC, B. RADICEVIC, K. KOVANDA, L. KOLAŘÍK, A. PETROVIC: 'Multi-objective calibration of the double-ellipsoid heat source model for GMAW process simulation', Therm. Sci., 26, pp. 2081-2092, 2022.
[14] J. M. CABEZA LAINEZ, J. A. PULIDO ARCAS, M.-V. CASTILLA, C. RUBIO BELLIDO, J. M. BONILLA MARTÍNEZ: 'Radiative Heat Transfer for Curvilinear Surfaces', in: S.R. Bello (Ed.), *Solar Radiation Applications*, InTech, 2015.
[15] G. TURICHIN, D. MUKIN, E. VALDAYTSEVA, M. SANNIKOV: 'Influence of Latent Heat of Fusion on the Melt Pool Shape and Size in the Direct Laser Deposition Process', *Materials*, Basel, Switzerland, 15, 2022.
[16] Y. SONG, Y. WANG, M. ZHANG: 'Experimental and Numerical Simulation on Laser welding of High Manganese TWIP980 Steel', *Procedia Manufacturing*, 37, pp. 385-393, 2019.
[17] J. S. T. LOOSE: *Leistungsmerkmale der Schweißstruktursimulation*, pp. 487-491, 2008.
[18] E. A. BONIFAZ, A. S. MENA: 'The Cooling Rate and Residual Stresses in an AISI 310 Laser Weld: A Meso-Scale Approach', *Crystals*, 12, 502, 2022.
[19] M. ZHANG, Y. ZHOU, C. HUANG, Q. CHU, W. ZHANG, J. LI: 'Simulation of Temperature Distribution and Microstructure Evolution in the Molten Pool of GTAW Ti-6Al-4V Alloy', *Materials*, Basel, Switzerland, 11, 2018.
[20] N. HEMPEL: *Zum Einfluss zyklischer Plastizität auf die Eigenspannungsentstehung beim Schweißen hochlegierter Stähle*, Shaker, 2022.
[21] L. SPIEß, G. TEICHERT, R. SCHWARZER, H. BEHNKEN, C. GENZEL: *Moderne Röntgenbeugung: Röntgendiffraktometrie für Materialwissenschaftler*, Physiker und Chemiker, Springer Spektrum Wiesbaden, 2019.